AIAA JOURNAL
Vol. 42, No. 9, September 2004

Dynamic Flow Response Due to Motion of Partial-Span Gurney-Type Flaps

Stephen A. Solovitz* and John K. Eaton†
Stanford University, Stanford, California 94305

Uninhabited air vehicles are commonly designed with high-aspect-ratio wings, which can be susceptible to significant aeroelastic vibrations. These oscillations can result in a loss of control or structural failure, and new techniques are necessary to alleviate them. A multidisciplinary effort at Stanford developed a distributed flow control method that used small trailing-edge actuators, known as micro-trailing-edge effectors (MiTEs) to alter the aerodynamic loads at specific spanwise locations along an airplane wing. The actuators were based on a Gurney flap, which is a trailing-edge flap of small size and large deflection, allowing an increase in lift with a small drag penalty. The transient response caused by relatively rapid MiTE actuation was studied using particle image velocimetry in the near wake. The transient response was quasi-steady for dimensionless actuation times (tU_∞/c) near unity. A shorter dimensionless actuation time of 0.2 produced a transient response with significant overshoot of the downwash velocity in the near wake. This indicated a nonmonotonic response of the aerodynamic loads for rapid actuation.

Nomenclature

b	=	wing span, 87.9 cm
C_L	=	coefficient of lift normalized by wing planform area, $L/(\frac{1}{2}\rho U_\infty^2 bc)$
c	=	airfoil chord length, 60.2 cm
L	=	lift
Re_c	=	Reynolds number based on chord length, $U_\infty c/\nu$
t	=	time after device actuation
t_{act}	=	flap actuation time, 28 ± 2 ms
t^*	=	nondimensional time, tU_∞/c
U_∞	=	flow velocity
u'	=	instantaneous streamwise fluctuation velocity
w'	=	instantaneous wing-normal fluctuation velocity
x	=	streamwise position (origin is at the airfoil leading edge)
z	=	wing-normal position (origin is at the chordline)
α_{app}	=	approximate downwash scalar
ν	=	kinematic viscosity
ρ	=	fluid density

Subscripts

max	=	maximum value of quantity
press	=	pressure side of airfoil
suct	=	suction side of airfoil
TE	=	trailing edge

Superscripts

$\sim$	=	phase-averaged quantity

Introduction

ACTIVE aeroelastic damping techniques, such as active wing structure or distributed flow control, offer the possibility of substantial aircraft performance improvement. This is particularly true for long-endurance aircraft with high-aspect-ratio wings, where passive techniques might not be sufficient in controlling high-order vibration modes. Such a vibratory mode led to the destruction of the Darkstar prototype, which had an aspect ratio of 15, in early 1996.[1] The present work is part of a multidisciplinary study to investigate the use of Gurney flaps as active control elements.

A Gurney flap is a small trailing-edge flap mounted at high deflection angle (typically 90 deg), which causes substantial changes in the lift and pitching moment. In our concept,[2] the Gurney flap is segmented into many small elements across the span. Each segment is called a micro-trailing-edge effector (MiTE). The MiTEs can be either two-state (up or down) or three-state (up, down, or neutral) actuators. Because the MiTEs are small, they can have very high bandwidth. The finite span of each flap limits the effect to a relatively small portion of the wing span. Therefore, it is possible to damp high-order vibration modes using a set of MiTEs distributed along the wing trailing edge.

The current effort is part of a collaborative research program that includes development of high bandwidth actuators,[3] measurement of the aerodynamic performance of the MiTEs,[4,5] and design of an autonomous aeroelastic damping system based on the MiTEs.[6] Our static aerodynamic measurements[4] have shown that MiTEs produce large changes in the lift and pitching moment, in good agreement with previous measurements[7] and computations.[8] Velocity field measurements[5] in the near wake of the flaps agreed well with the flow configuration postulated by Liebeck,[9] detailed laser Doppler anemometry (LDA) measurements by Jeffrey et al.,[7] and computational fluid dynamics analysis by Jang et al.[8] The MiTE lift increment varied linearly with actuated span down to the smallest aspect ratios tested (similar to other experiments[10,11]). This response was independent of flap pattern, as the increments superposed linearly for configurations both with and without gaps between MiTEs. More recent work[5] demonstrated that the device effects were primarily localized within two flap spans. Hence, the effects of the MiTEs could be modeled very simply when they are static, as they provide a known load to a specific location along the wing.

The use of segmented Gurney flaps in an aeroelastic control system requires high frequency actuation, especially if higher-order vibration modes are of concern. Previous static experiments have shown that Gurney flaps produce sufficient control response and can be modeled simply, making them potential candidates for aeroelastic control actuators. What is not known is the dynamic response caused by rapidly actuated MiTEs. To date, there have been no externally reported measurements or simulations of rapidly actuated Gurney flaps. The goals of the present work were to examine the dynamic response of the flow for fast MiTE motion. Actuation was

Received 13 March 2003; revision received 4 February 2004; accepted for publication 17 April 2004.

*Graduate Research Assistant, Department of Mechanical Engineering; currently Mechanical Engineer, General Electric Global Research, One Research Circle, ES107, Niskayuna, NY 12309.

†Professor, Department of Mechanical Engineering, 488 Escondido Mall, Building 500, Room 501F. Senior Member AIAA.

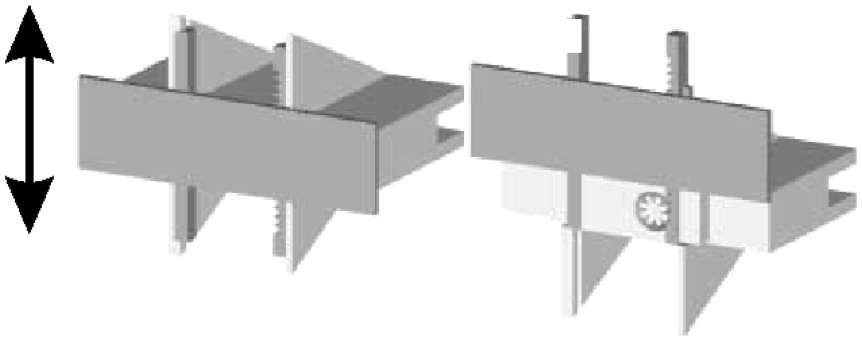

a)

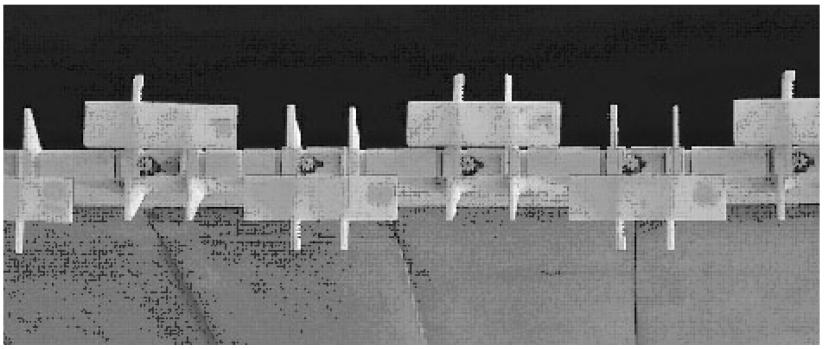

b)

Fig. 1 MiTE design; a) schematic of MiTE actuator (9-mm flap height) and b) image of a series of MiTEs attached to the airfoil trailing edge.

studied for two dimensionless frequencies: one near the boundary of quasi-static behavior and one at a significantly higher frequency.

Experimental Apparatus

The experiments were performed in the Stanford Flow Control Wind Tunnel, a subsonic (0–22 m/s) closed-loop wind tunnel with excellent flow uniformity and freestream turbulence below 0.5%. The test section is 61 cm wide $\times$ 91 cm high $\times$ 4 m long.

A two-dimensional airfoil model with a MESO5 profile was mounted vertically in the test section, spanning the tunnel height. The chord length, including a blunt manifold for MiTE attachment, was $c = 60.2$ cm. Boundary-layer trips were installed 12.6% of the chord length downstream of the leading edge on both the suction and pressure surfaces to provide uniform transition to turbulence.

Sixteen MiTE actuators were attached to the blunted trailing edge about the spanwise midpoint. Each MiTE had a 31-mm span. When actuated, the devices extended from the wing surface by 9 mm, corresponding to 1.5% of the wing chord. (The MiTEs were designed and constructed by B. Park in the Stanford Rapid Prototyping Laboratory. Details of their development and manufacturing are described in his dissertation.[3]) A small dc motor drove each flap via a rack-and-pinion linkage, as shown in Fig. 1. Each flap was controlled by an independent one-bit digital line from the laboratory computer, which allowed motion between the fully up and fully down positions in approximately 30 ms. Thus, the devices could be operated at frequencies in excess of 17 Hz while still achieving full extension in each direction. The motion was very repeatable, as demonstrated next.

The MiTEs had only two possible positions during dynamic operation. A third, neutral position, achieved by fixing the flap behind the blunt trailing edge, was also used during static tests. In this position, the flap protruded from the blunted edge by 1.25 mm on both sides. The 16 adjacent, functional flaps did not span the entire wing, only occupying the central 48 cm. To simulate uniform actuation in one direction, stationary flaps with the same 9-mm chord length could be mounted over the remainder of the span.

The flow structure in the near wake was examined by particle image velocimetry (PIV) interrogation with a commercial TSI system. A Spectra-Physics Nd:YAG PIV 400 dual-head laser was used to illuminate the test region. The laser was located outside of the tunnel, and then its beam passed through an articulated arm to the laser-sheet optics. These optics produced a laser sheet just downstream of the trailing edge, centered on a midspan MiTE. The image window extended about 7% of the chord past the wing and $\pm 2.5\%$ of the chord on either side. The flow was seeded with a Rosco Delta 3000 fog generator, which was located in the downstream end of the test section, approximately 3 m past the wing. The generator vaporized a glycerol, which produced a fine mist of droplets on the order of 0.3 μm in diameter. After circulating back through the tunnel blower, these particles were uniformly dispersed in the interrogation region. The region was imaged with a TSI PIVCAM 13-8 charge-coupled device (CCD) camera, which was positioned beneath the tunnel. The PIV system was controlled by a synchronizer, which was operated using Insight software. The PIV analysis was performed with Pivlab2000, an iterative processing program developed by D. Han.[12] In this configuration, the smallest interrogation region was 0.6×0.6 mm, and the uncertainty in measured velocity was $\pm 0.9\%$. The uncertainty in the Reynolds normal stresses was $\pm 13\%$.

The actual motion of an actuated MiTE was examined by using phase-locked, strobed digital imaging. A strobe light was externally triggered at a specific time interval after the microflap was actuated. The CCD camera acquired images of the device when it was illuminated. The flap position was measured by determining the pixel locations of its edges in these images. By varying the trigger interval of the strobe light, the entire flap motion was attained. This same technique was used to trigger the PIV measurements so that the flow response could be determined.

Figure 2 displays the flap position at various times after the MiTE was actuated, compiled from an average of 500 images at each phase. There are two sets of data illustrated here: one with no tunnel flow and one with the tunnel at the maximum speed of 22 m/s. Both cases exhibited the same response, with the flap moving monotonically

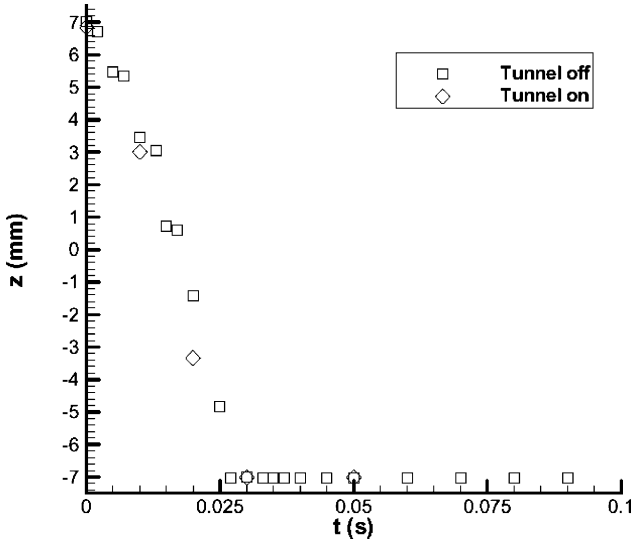

Fig. 2 Actuator position vs time for up-to-down motion.

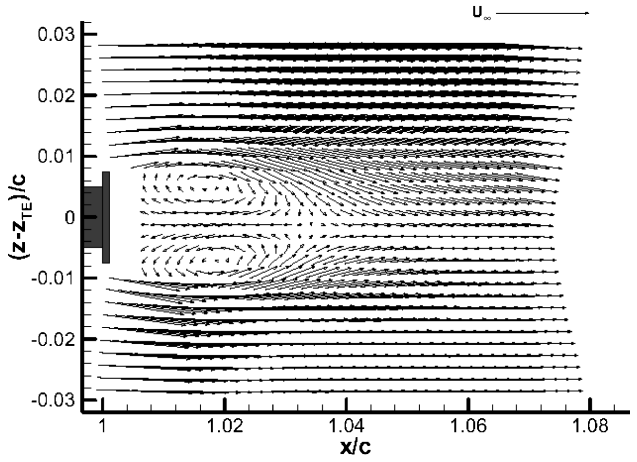

Fig. 3 Mean flow velocity field for the full-span neutral position.

from up to down in approximately $t_{act} = 28 \pm 2$ ms. The position was nearly linear with time. Given the response interval, the maximum MiTE frequency was on the order of 18 Hz. Note that there was some slight variation between individual images caused by jitter in the actuator. The maximum deviation was on the order of 10% of the actuator height.

Results

Full-Span Actuation

The initial experiments considered static situations, which were the only cases where the flow structure had been studied quantitatively in previous research.[5,7] The wing was oriented at an angle of attack of 0.57 deg, and the Reynolds number was fixed at $Re_c = 9.0 \times 10^5$. For each condition, 1000 image pairs of PIV data were acquired.

Figure 3 shows the mean velocity vectors when all of the MiTEs were in the neutral position, obtained by ensemble averaging all 1000 measured velocity fields. In the mean, the separated flow contains two counter-rotating vortices of similar size and strength. This basic structure is very similar to that expected for blunt trailing edges.[13]

For the full-span down position, all MiTEs and fixed flaps were actuated toward the pressure surface. The mean flowfield is given in Fig. 4, which shows a larger separated region and turning of the flow towards the pressure side. This turning indicates greater circulation and lift. The pair of counter-rotating vortices was still present, but their locations and shapes were different. The suction-side vortex was larger and located near the wing, whereas the pressure-side vortex was smaller and shifted off of the surface. This time-averaged flow was comparable to the postulated flow of Liebeck,[9] the computations of Jang et al.,[8] and the LDA experiments of Jeffrey et al.[7]

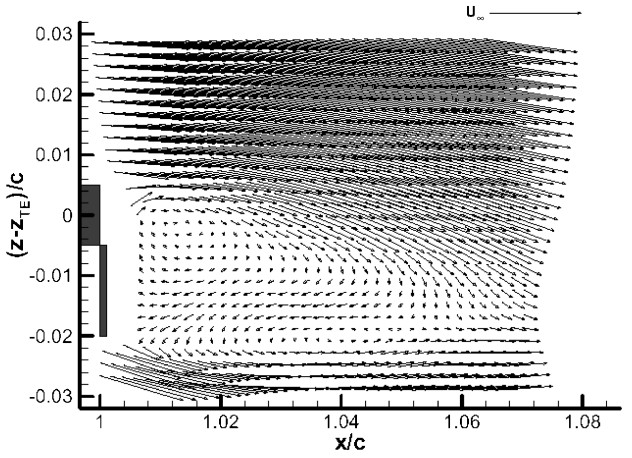

Fig. 4 Mean flow velocity field for the full-span down position.

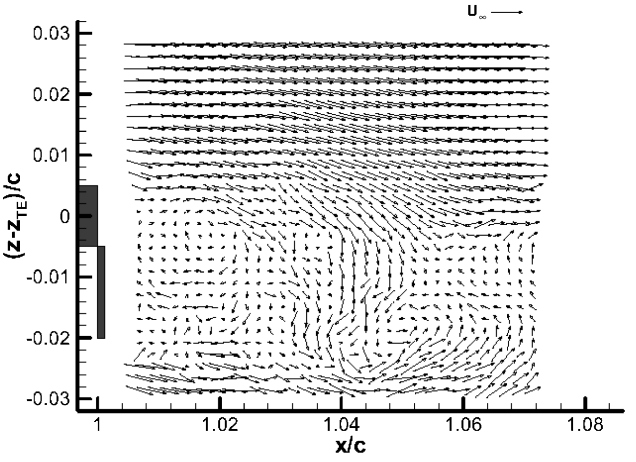

Fig. 5 Typical instantaneous velocity field for the full-span down position.

Note that the individual instantaneous vector plots did not show the same clear vortical structures. In each instantaneous field, there were large vortices similar to the bluff-body shedding seen by Jeffrey et al.,[7] alternating in sign and offset in location. The individual PIV fields were not phase locked to the flow, so that each image showed different, random phases of the shedding. Figure 5 shows an image where the suction-side vortex is still attached to the wing, while the pressure-side vortex has been shed. It was not possible to simultaneously view two shed vortices because of the window size, and so a Strouhal number could not be determined from these PIV realizations.

Single MiTE Actuation

Dynamic tests studied the aerodynamic response to a single actuated flap centered on the midspan location while all other flaps were held neutral. Note that in application, MiTEs will usually be actuated independently. Also, because of the slight jitter it was not possible to move all 16 actuated flaps at precisely the same instant. In the static case, the mean flow structure at the center of a single MiTE was qualitatively similar to the full-span down case, as shown in Fig. 6. The time-averaged field exhibited downturned flow, a larger separated region, and a more prominent suction-side vortex. There were differences between the cases, as the two vortices had slightly different sizes and shapes, and there was a larger downwash in the partial-span case. Still, the qualitative similarity suggests that the transient variation should be comparable.

The maximum wing-normal Reynolds normal stress is a useful quantitative statistic for examining the dynamic response. Figure 7

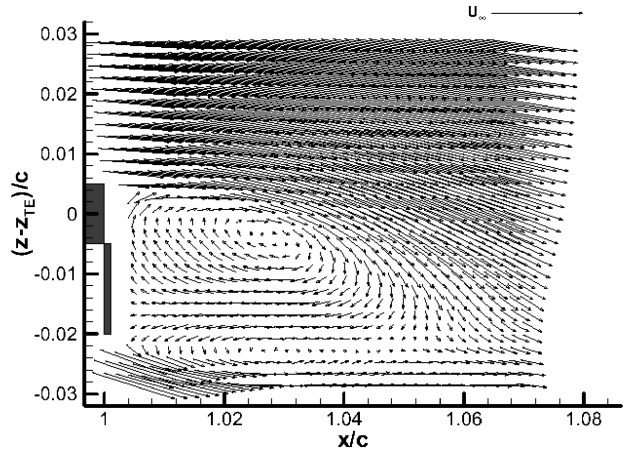

Fig. 6 Mean flow velocity field for a single actuated MiTE at midspan with all other MiTEs held neutral.

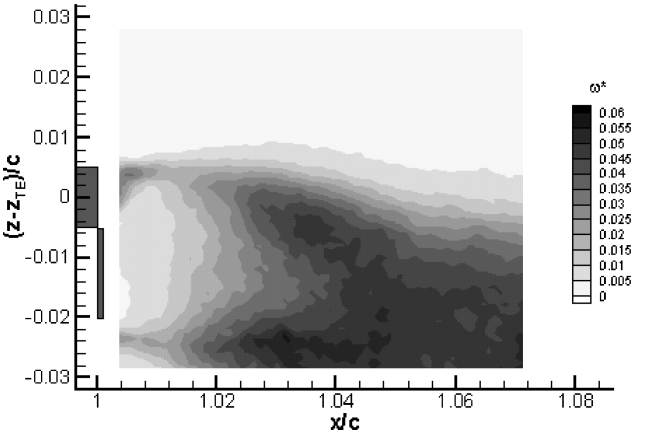

Fig. 7 Mean flow wing-normal Reynolds-stress field for a single actuated MiTE at midspan with all other MiTEs held neutral.

shows the wing-normal Reynolds-stress distribution for a single midspan MiTE fixed downward. The peak in the distribution is located at approximately $x/c = 1.05$ and $(z - z_{TE})/c = -0.025$, which is near the off-surface stagnation point. This location is typical of bluff-body shedding, as is the peak value of 0.059. Note that the streamwise Reynolds normal stress (not displayed) showed two peaks near the off-surface stagnation point, which is also representative of a bluff-body flow.

Dynamic Actuation

The first dynamic tests were conducted at the maximum Reynolds number of 9.0×10^5. The moving MiTE was actuated in a 1-Hz square wave, which had a timescale far above the flap actuation t_{act} and aerodynamic c/U_∞ times. A total of 500 samples were acquired for each phase, and these were phase averaged to determine the mean and fluctuating velocity statistics. The phase-averaged flow structures for nondimensional times $t^* = 0$, 0.37, 0.73, 1.10, and 1.46 are shown in Fig. 8. The flap actuation time corresponded to about $t^* = 1.03$.

At $t^* = 0$, shown in Fig. 8a, the MiTE was in the up position, and the flow structure was basically the opposite of the single flap down case seen in Fig. 6. There was a significant upwash downstream of the flap, and the pressure-side vortex was the stronger of the counter-rotating pair. In the next phase, $t^* = 0.37$, displayed in Fig. 8b; the flap had moved about one-third of the way to the down position. The counter-rotating vortex pair had shrunk in size and strength, and the off-surface stagnation point was closer to the wing and more towards the pressure side. The flap began to extend past the airfoil pressure surface at $t^* = 0.73$, shown in Fig. 8c. The vortex pair was still just behind the flap, and the off-surface stagnation point had moved with it toward the pressure side. The suction-side vortex had grown in size relative to the pressure-side eddy, and it had also moved nearer to the trailing edge.

The MiTE had reached the down position at the next phase, $t^* = 1.10$, given in Fig. 8d. As before, the counter-rotating pair was immediately behind the flap, and the vortices had begun to grow in extent. The off-surface stagnation point was further downstream and more toward the pressure side. The suction-side vortex was now much larger in size. The wake had not completely developed by this phase, as the size of the separated region was still smaller than in the static condition. However, the structure was already very similar to the static structure for a single flap down. By the final phase, $t^* = 1.46$, displayed in Fig. 8e, the wake had reestablished the static condition, becoming nearly identical to the static flow structure in Fig. 6.

The response for this nondimensional actuation time ($t^*_{act} = 1.03$) was nearly quasi-steady. Instantaneous fields at $t^* = 0$ and 0.37 showed no coherent response. Apparently, random images of bluff-body shedding were observed, with no eddy phase coherence between different images. At $t^* = 0.73$, there was weak evidence of phase-locked response. Note that at this time the flap was moving rapidly into the pressure-side stream. The same flow pattern observed in the phase average (Fig. 8c) was seen in every instantaneous realization. This indicates that vorticity shedding was phase locked by the rapid flap motion. However, by the time the flap reached full extension ($t^* = 1.10$) the vortex shedding was no longer phase locked.

Although the phase-averaged response appeared quasi-steady except around $t^* = 0.73$, there was actually significant phase lag in the final development of the wake. The wake at $t^* = 1.10$ was similar to the steady case, but the separated region was still smaller than in that static condition. The recovery of the flow was essentially complete by $t^* = 1.46$.

These qualitative conclusions were verified using quantitative measures of the flow statistics. Table 1 contains the maximum value of the phase-averaged, wing-normal Reynolds normal stress, as well as an approximate measure of the downwash α_{app}. The value of α_{app} was determined by finding the angle of the average velocity vector at $x/c = 1.060$, a location generally downstream of the recirculating bubble. This value was not assumed to be the actual downwash angle, as the imaged region only covered a portion of the wake. The scalar was simply meant to be a quantitative value for comparative purposes. The uncertainty in α_{app} is $\pm 0.9\%$. Overall, the quantitative parameters indicate that the wake gradually changed in time as the flap moved. There is a noticeable increase in the peak wing-normal stress at $t^* = 1.10$ compared to the static case, which suggests that stronger vortices were shed immediately after the flap reached the down position, even though the flow was not perfectly phase locked with the flap motion. The peak stress returned to the static levels by the next phase, though. Note that the statistics for the static up and down positions were not equal in magnitude, as the airfoil was asymmetric.

It is not surprising that the response is nearly quasi-steady for a dimensionless actuation time near one. The change in flap position creates an increase in the clockwise circulation around the wing, which must be accompanied by the shedding of counterclockwise circulation from the trailing edge. For an instantaneous change in the geometry, one would expect the shedding of a single large counterclockwise vortex. However, if bluff-body shedding were occurring much more rapidly than the flap motion the counterclockwise

Table 1 Quantitative measures of flow response caused by dynamic actuation: $t^*_{act} = 1.03$

t^*	α_{app}, deg	$\widetilde{w'^2}_{max}/U_\infty^2$
0	9.9	0.049
0.37	5.2	0.049
0.73	−3.3	0.047
1.10	−15.4	0.098
1.46	−15.5	0.062
2.55	−15.9	0.052

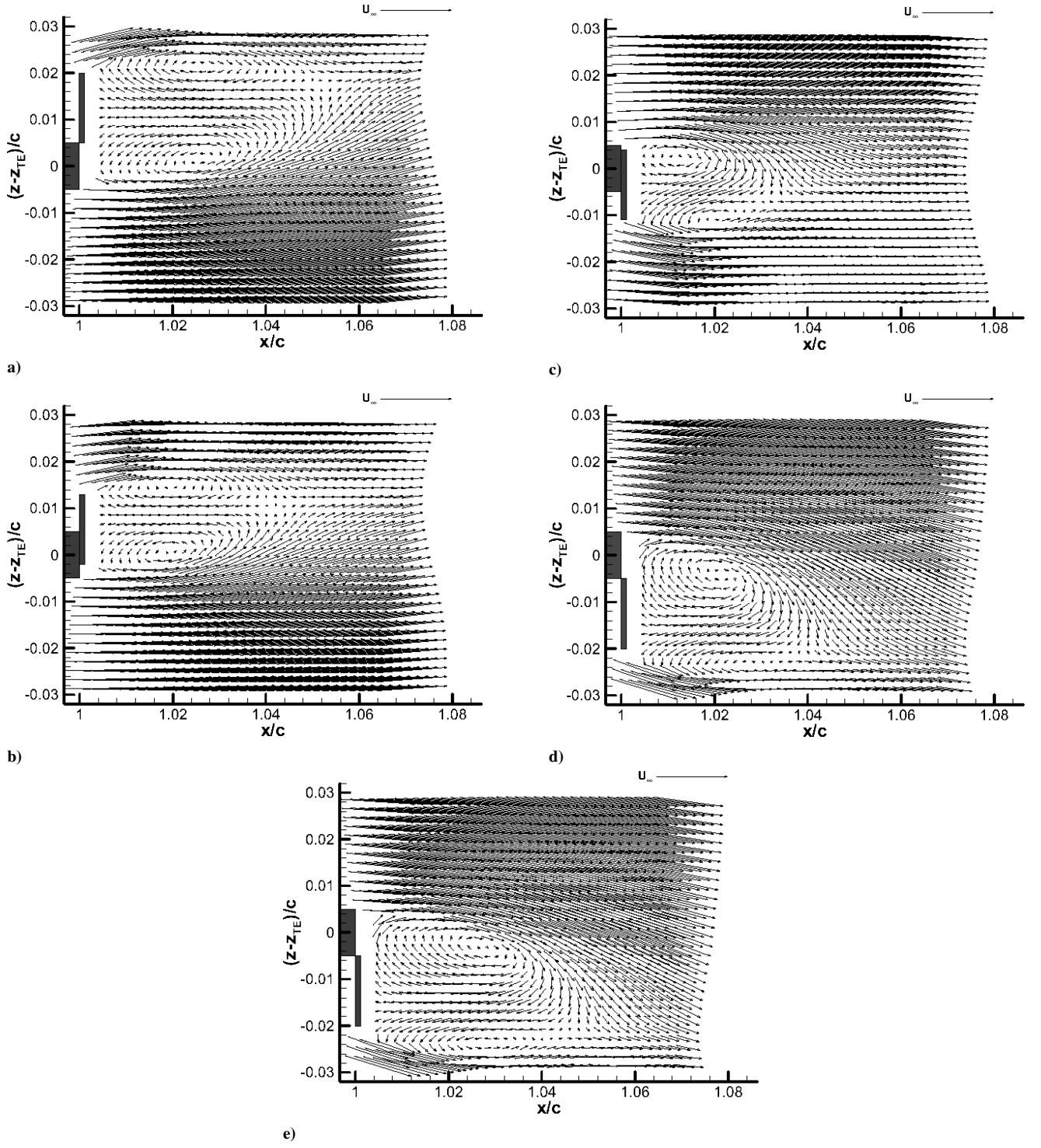

Fig. 8 Phase-averaged velocity field during dynamic actuation at U_∞ = 22.0 m/s: t^*_{act} = a) 0, b) 0.37, c) 0.73, d) 1.10, and e) 1.46.

circulation would be shed incrementally. Assuming a Strouhal number of 0.2 and a thickness scale of 1 cm, approximately 12 vortices would be shed during the 28-ms actuation time. Each of these shed vortices would carry part of the overall circulation change, and thus the flow would adjust gradually. The most rapid circulation change occurred around $t^* = 0.73$, resulting in a strong coherent shed vortex at that phase.

A second, much shorter dimensionless actuation time was tested in order to examine the response when the flow was far from quasi-steady. Because the maximum actuation rate was fixed, the only way to do this was to reduce the freestream velocity, raising the convective timescale. The Reynolds number was lowered to 1.8×10^5, which increased the aerodynamic response time to 137 ms. The vortex shedding time was on the order of 11 ms, which meant that only three vortices were shed during the actuation time. At this reduced Re_c, the flow should no longer be turbulent over much of the airfoil, and thus the response should be somewhat different than with the previous experiments. However, the Gurney flap effect is inviscid in nature, as the lift alteration is primarily because of a change in the Kutta condition. Hence, the first-order dynamic response should be comparable. Also, the previously reported static measurements showed only a slight effect of Reynolds number in this range.

The phase-locked average response was determined for a number of time intervals. Figure 9 displays the phase-averaged velocity fields for eight different phases between $t^* = 0$ and 0.44. This range completely covered the transient response to the MiTE actuation.

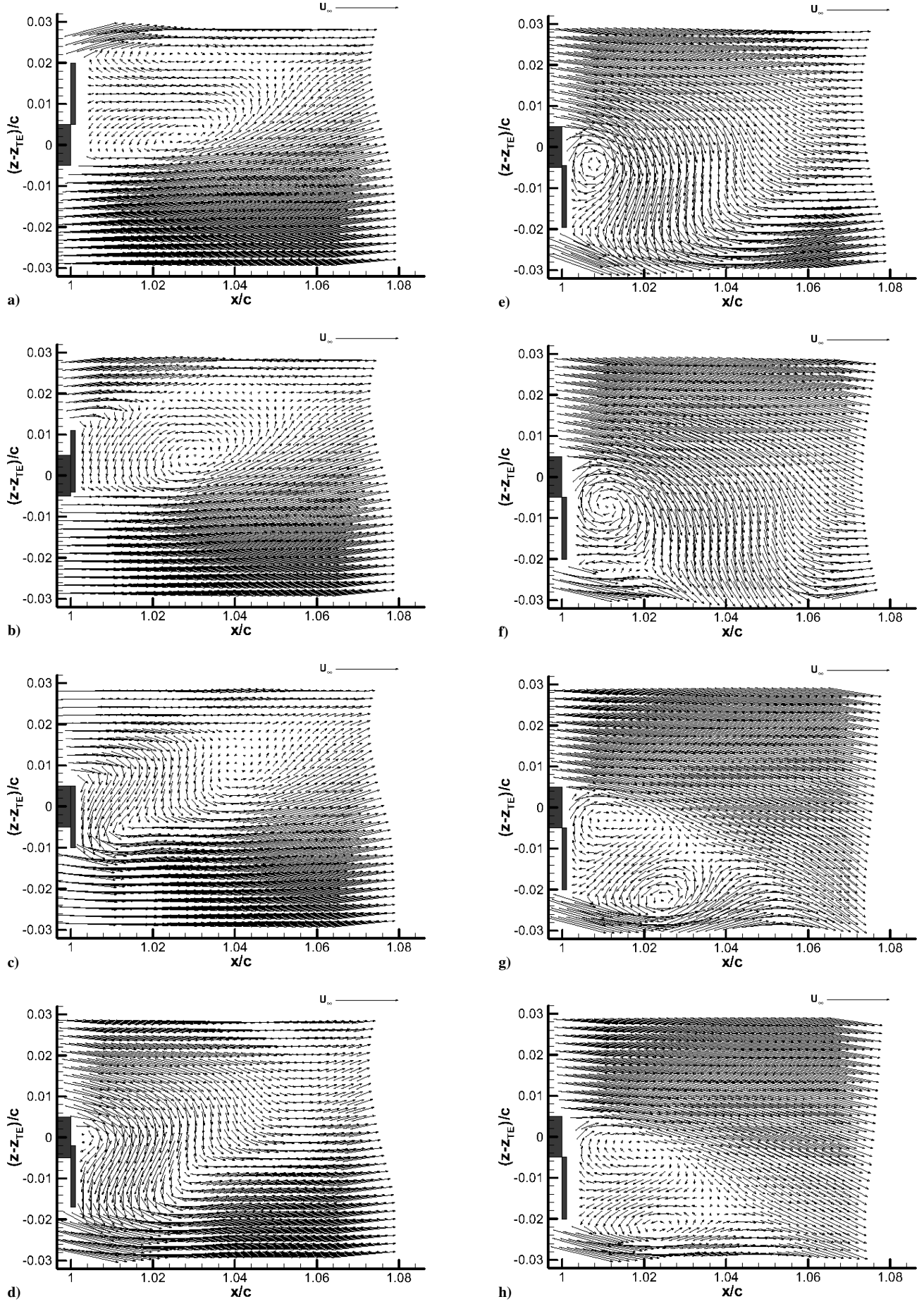

Fig. 9 Phase-averaged velocity field during dynamic actuation at U_∞ = 4.4 m/s: f^*_{act} = a) 0, b) 0.07, c) 0.11, d) 0.15, e) 0.18, f) 0.22, g) 0.29, and h) 0.44.

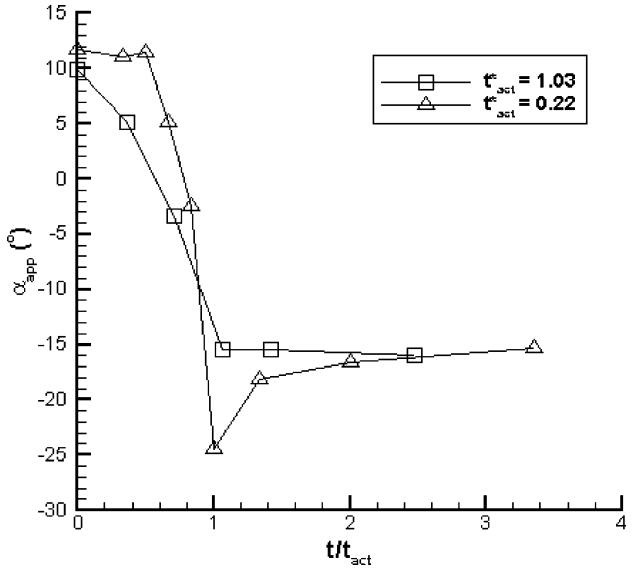

Fig. 10 Comparison of approximate downwash responses for $t^*_{act} = 0.22$ and 1.03.

At $t^* = 0$, the flow structure shown in Fig. 9a was comparable to that seen for the longer t^*_{act} tests, as would be expected. Once the flap began to move, the wake development deviated from the high-speed experiments. Prior to the flap motion, the wake consisted of bluff-body shedding, and each instantaneous image showed a random configuration of the alternating vortices being shed and developed. At $t^* = 0.07$ (Fig. 9b), the MiTE had moved far enough that the wake on the suction side was exposed to the freestream velocity, and this low-velocity region of the wake was convected downstream. Thus, the clockwise vorticity was immediately shed, regardless of its stage of development. This is seen in the phase-averaged flow, as the suction-side vortex moved further past the trailing edge and decreased in size. The pressure side of the separated region was still obstructed from the freestream by the moving flap, so it did not move far downstream or decrease much in size. The counterclockwise vorticity at the pressure side of the wake entrained flow from the suction side downward, parallel to the flap surface. Once this entrained fluid encountered the freestream flow on the pressure side, it turned and moved along with the freestream.

Because the clockwise vorticity on the suction side was shed for every case, the counterclockwise vortex dominated in measurement of this phase. Thus, the near wake became phase locked to the motion of the flap. This is evident when comparing instantaneous plots, which showed downward flow parallel to the flap in every processed image. Farther downstream of the wing, the flow was not phase locked, as the suction-side vortex was in a random state of development when the device began to move.

At later phases, the flow very near the flap remained coherent for every instantaneous image, whereas the structures farther downstream were random. Figure 9c shows the phase-averaged flow at $t^* = 0.11$. By this phase, the original suction-side vortex was no longer observed, being completely shed from the surface. The pressure-side vortex was now fully exposed to the suction-side freestream flow, so that it was convected farther downstream. The coherent near wake continued to follow the airfoil contour.

By $t^* = 0.15$, the original wake was no longer present (see Fig. 9d), having been shed from the wing. Near the flap, the entrainment along the MiTE surface continued, but a small separated region began to form near the edge of the suction surface. This vortex continued to grow at $t^* = 0.18$, as seen in Fig. 9e. The increased clockwise circulation had a clear effect on the freestream flow, adding a strong downwash. The flow turning was even more apparent by $t^* = 0.22$, as fluid moved downward out of the image window in Fig. 9f. The flap was fully down at this phase, and the developing clockwise vortex now occupied much of the region just

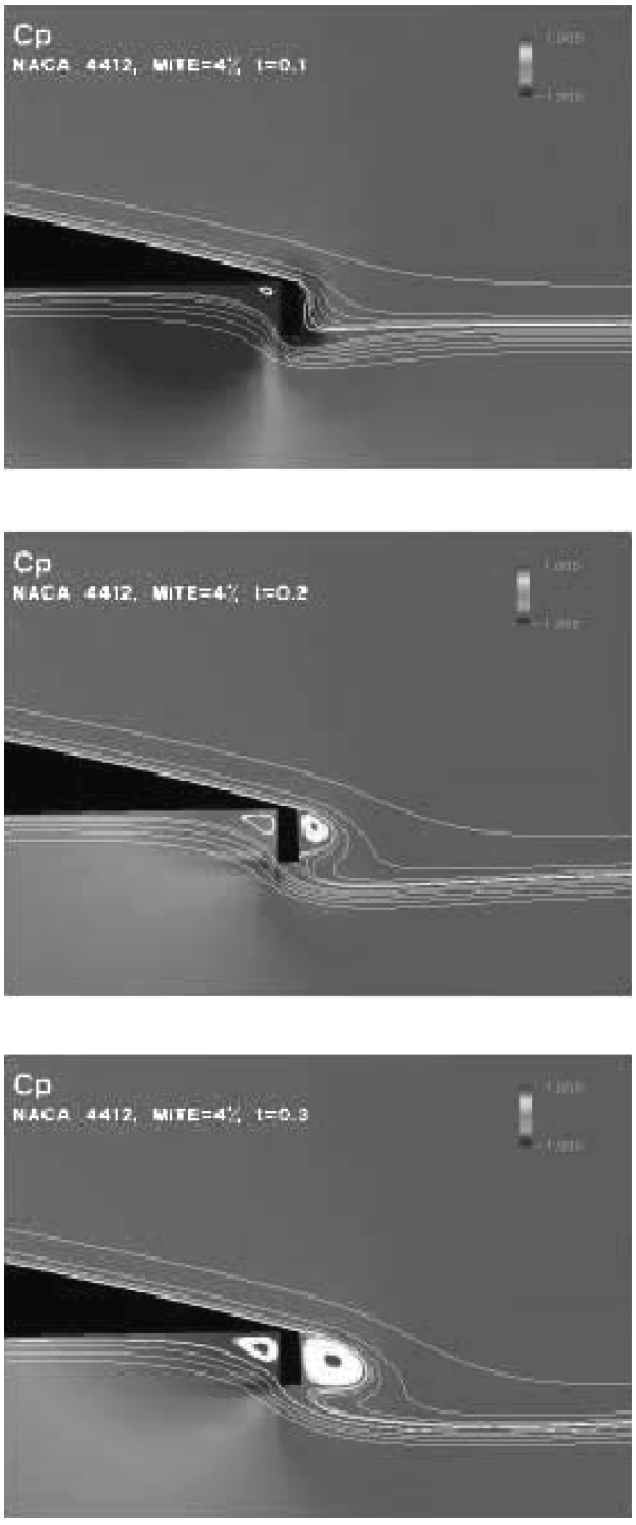

Fig. 11 Predicted phase-averaged streamlines during dynamic actuation at $t^*_{act} = 0.1$, 0.2, and 0.3 (Kroo et al.[14]).

downstream of the actuator. When the fluid rotating around this vortex encountered the freestream on the pressure side, it was quickly accelerated in the downstream direction, showing a rapid counterclockwise turning. This produced a tiny counterclockwise vortex at the tip of the flap. As this vortex grew, the wake structure began to develop toward the final, static condition. Figure 9g shows the phase-averaged flow at $t^* = 0.29$, where the pair of vortices had grown to approximately the same size. Unlike the static case, these two structures were coherent. The pressure-side vortex was stronger compared to the preceding phase, which reduced the downwash.

Table 2 Quantitative measures of flow response caused by dynamic actuation: $t^*_{act} = 0.022$

t^*	α_{app}, deg	$\widetilde{w'^2}_{max}/U^2_\infty$
0	11.7	0.048
0.073	11.1	0.039
0.110	11.5	0.048
0.146	5.1	0.058
0.183	−2.5	0.061
0.220	−24.4	0.077
0.293	−18.1	0.080
0.440	−16.6	0.073
0.739	−15.3	0.057

This suggests that a transient lift measurement at this speed would show a spike.

Figure 9h displays the phase-averaged velocity field at $t^* = 0.44$, which is comparable to the wake structure seen in the static condition. The vortical structures were no longer the same in every image, indicating that bluff-body shedding had begun to dominate once again. Thus, the transient response to actuation was mostly complete at this phase. For later times, the structure did not change significantly.

The quantitative results for the short t^*_{act} experiments are shown in Table 2. This further demonstrates the spike that occurs in the transient response, particularly evident in the downwash. Figure 10 compares the approximate downwash response for the two dimensionless actuation times. In this plot, the time following actuation t is nondimensionalized by t_{act}, as this parameter is identical for the two cases. Both situations have similar values of α_{app} initially, and they each reach the same final level after the response settles. However, in between the downwash response differs greatly. For t^*_{act} near unity, α_{app} decreases monotonically, reaching the final state a short time after the actuation is complete. For the lower t^*_{act}, the downwash scalar does not change immediately, and then it turns strongly downward, beyond the final value of α_{app}. After this spike, the response settles back to the static condition.

This spike in α_{app} can be used to provide a preliminary estimate of the lift overshoot magnitude. Earlier measurements[4] indicated that C_L changes by about 0.5 between the static full-span up and down positions. The PIV measurements for these cases showed a corresponding change in α_{app} of about 30 deg. For the low t^*_{act} case, the downwash spike is approximately 9 deg, suggesting a lift overshoot of $\Delta C_L \approx 0.5*(9 \text{ deg}/30 \text{ deg}) = 0.15$, which is a significant effect. Admittedly, this is only an estimate of the actual ΔC_L, as α_{app} is simply a scalar that behaves similarly to the downwash, not an exact measure of it. In addition, the dynamic experiments used a single MiTE rather than full-span actuation, and so the overall change in α_{app} is only an approximation. Even so, this does suggest that the lift overshoot is not negligible.

The transient response was comparable to computations for a dynamic MiTE performed by S. Elkayam (see Ref. 14). These calculations considered a NACA 4412 airfoil with a sharp trailing edge. Figure 11 shows the predicted flow structure at nondimensional times $t^* = 0.1$, 0.2, and 0.3, which clearly shows the growth of the counter-rotating vortices observed in Figs. 9c–9g. The agreement is remarkable, particularly because these computations modeled the flap actuation as instantaneous between the up position and the down position. For the small t^*_{act} experiments, this assumption was valid, as the convective timescale was considerably larger than the actuation time. At higher speed, the timescales were of the same order, and the measured flow structure did not correspond to the computations.

Conclusions

The aerodynamic response to micro-trailing-edge-effector (MiTE) actuation can be modeled very simply. The devices produce a localized lift response that is linearly dependent on actuated span, regardless of configuration. This effect is nearly quasi-steady for dimensionless actuation times ($t^*_{act} = tU_\infty/c$) near unity. The experiments showed that the wake followed the flap as it changed position. Phase-locked vortex structures were weak and produced no significant lift overshoot. The wake quickly relaxed to its steady-state configuration shortly after completion of the actuation. This quasi-steady response occurred because the MiTE actuation time was significantly larger than the bluff-body vortex shedding period for the flaps. The starting vorticity produced by the change in airfoil circulation was shed incrementally as part of the vortex-shedding process, rather than as a single coherent vortex.

Dimensionless actuation times near unity are probably practical for flight conditions. Considering a wing chord of 2 m and a flight speed of 100 m/s (approximately 220 mph), actuation times of 20 ms would be required. Actuation times of this order appear to be practical, given flap sizes of a few centimeters. Faster actuation might be possible with advanced actuator design. Also, faster dimensionless actuation times might be found with a large wing chord or with low speed aircraft.

For dimensionless actuation times below unity, the present results indicate that a quasi-steady analysis cannot be applied to the controller design. There was already a small amount of phase lag in establishing the steady wake for t^*_{act} near one. At the faster dimensionless actuation time ($t^*_{act} = 0.22$), there was a strong coherent response, including substantial lift overshoot. If very high bandwidth actuators were developed, these transient aerodynamic effects would have to be considered.

Acknowledgments

This work was sponsored by the Air Force Office of Scientific Research. The collaborations of Ilan Kroo, Fritz Prinz, Byong-ho Park, Hak-tae Lee, Stefan Bieniawski, and Claude Matalanis were critical to the research.

References

[1]Dornheim, M. A., "DarkStar Destroyed on Second Flight," *Aviation Week and Space Technology*, Vol. 144, No. 18, 1996, pp. 24, 25.

[2]Kroo, I. M., "Aerodynamic Concepts for Future Aircraft," AIAA Paper 99-3524, June–July 1999.

[3]Park, B., "Miniaturization of Functional Mechanisms with SDM Processing," Ph.D. Dissertation, Dept. of Mechanical Engineering, Stanford Univ., Stanford, CA, Feb. 2002.

[4]Solovitz, S. A., and Eaton, J. K., "Experimental Aerodynamics of Mesoscale Trailing-Edge Actuators," *AIAA Journal*, Vol. 40, No. 12, 2002, pp. 2538–2540.

[5]Solovitz, S. A., and Eaton, J. K., "Spanwise Response Variation for Partial-Span Gurney-Type Flaps," *AIAA Journal*, Vol. 42, No. 8, 2004, pp. 1640–1643.

[6]Lee, H., Kroo, I. M., and Bieniawski, S., "Flutter Suppression for High Aspect Ratio Flexible Wings Using Microflaps," AIAA Paper 2002-1717, April 2002.

[7]Jeffrey, D., Zhang, X., and Hurst, D. W., "Aerodynamics of Gurney Flaps on a Single-Element High-Lift Wing," *Journal of Aircraft*, Vol. 37, No. 2, 2000, pp. 295–301.

[8]Jang, C. S., Ross, J. C., and Cummings, R. M., "Computational Evaluation of an Airfoil with a Gurney Flap," AIAA Paper 92-2708, June 1992.

[9]Liebeck, R. H., "Design of Subsonic Airfoils for High Lift," *Journal of Aircraft*, Vol. 15, No. 9, 1978, pp. 547–561.

[10]Myose, R., Papadakis, M., and Heron, I., "Gurney Flap Experiments on Airfoils, Wings, and Reflection Plane Model," *Journal of Aircraft*, Vol. 35, No. 2, 1998, pp. 206–211.

[11]Nakafuji, D., van Dam, C., Michel, J., and Morrison, P., "Load Control for Turbine Blades: A Non-Traditional Microtab Approach," AIAA Paper 2002-0054, Jan. 2002.

[12]Han, D., "Study of Turbulent Nonpremixed Jet Flames Using Simultaneous Measurements of Velocity and CH Distributions," Ph.D. Dissertation, Dept. of Mechanical Engineering, Stanford Univ., Stanford, CA, March 2001.

[13]Stanaway, S., McCroskey, W. J., and Kroo, I., "Navier–Stokes Analysis of Blunt Trailing Edge Airfoils," AIAA Paper 92-0024, Jan. 1992.

[14]Kroo, I. M., Eaton, J. K., and Prinz, F., "UAV Aeroelastic Control Using Redundant Microactuators," Air Force Office of Scientific Research, Program Review for Year I, TR-99-0252, Stanford, CA, 1999.

E. Livne
Associate Editor